Sea ice salinity and structure: A winter time series of salinity and its distribution

A. J. Gough,[1] A. R. Mahoney,[2] P. J. Langhorne,[1] M. J. M. Williams,[3] and T. G. Haskell[4]

Received 18 August 2011; revised 28 December 2011; accepted 9 January 2012; published 8 March 2012.

[1] We present a winter time series of Antarctic sea ice salinity from eastern McMurdo Sound, an area close to an ice shelf where a subice platelet layer forms below the sea ice late in winter. This dramatically changes the sea ice structure as the sea ice grows into the subice platelet layer. Every 2 weeks during the 5 months of sea ice formation, salinity profiles were measured, along with detailed measurements of ice structure and growth rates. Once the influence of growth rate on sea ice bulk salinity is removed, the data from 69 cores and the results of a basic parameterization demonstrate that bulk salinity for platelet ice is higher than that for columnar sea ice. We also present measurements of the salinity profile close to the ice-water interface and use these to investigate the expected regime of fluid flow within the permeable portions of the sea ice, with particular reference to mushy layer and percolation theory. Finally, we provide a new distribution of sea ice salinity from 740 measurements, which can be interpreted as the sum of two spatial fields that we attribute to sea ice samples with and without brine channels and which should be reproduced by any realistic sea ice models. This distribution suggests that two measurements of quantities linearly linked to sea ice salinity must differ by 29% if they are to be considered different with 90% confidence.

Citation: Gough, A. J., A. R. Mahoney, P. J. Langhorne, M. J. M. Williams, and T. G. Haskell (2012), Sea ice salinity and structure: A winter time series of salinity and its distribution, *J. Geophys. Res.*, *117*, C03008, doi:10.1029/2011JC007527.

1. Introduction

[2] Sea ice is a composite material consisting of brine within a matrix of pure ice crystals [*Weeks*, 2010]. The bulk salinity of sea ice at the end of winter is important as it determines its thermal and mechanical properties [*Pringle et al.*, 2007; *Weeks*, 2010], and because brine carries the nutrients necessary for biological activity as spring begins [e.g., *Arrigo et al.*, 1993; *Vancoppenolle et al.*, 2010].

[3] Growing sea ice rejects brine to the ocean [e.g., *Malmgren*, 1927]. Any brine within sea ice is contained in millimeter to centimeter scale enclosures and tubes between the crystals of recently formed sea ice. These provide a route for dense brine to leave the ice [*Assur*, 1958; *Bennington*, 1967; *Eide and Martin*, 1975; *Niedrauer and Martin*, 1979]. As these networks close off, their remnants are the small (<1 mm) brine inclusions that determine many of the physical properties of the sea ice. These brine inclusions are oriented in a similar way to the crystals themselves [*Weissenberger et al.*, 1992; *Eicken et al.*, 2000]. The largest brine-filled remnants, brine drainage channels, have diameters up to a few millimeters [*Lake and Lewis*, 1970]. Once the freezing front has passed a given layer of sea ice, its temperature and salinity decrease. Freezing in the brine enclosures causes the porosity to decrease until eventually desalination at that level ceases [*Nakawo and Sinha*, 1981; *Backstrom and Eicken*, 2006]. Brine is then trapped for the remainder of the growth season so that a typical salinity profile evolves as sketched in Figure 1. The precise shape of the profile depends on conditions during growth, which can vary over the winter [*Eicken*, 1992].

[4] In spite of the importance of salinity as a pivotal parameter few studies exist where more than a handful of closely spaced cores have been taken from sea ice, and fewer still during the winter. Our intuition suggests that there is considerable variability in salinity because of the inhomogeneous distribution of brine, but we cannot easily quantify this. *Weeks and Lee* [1962] produced a distribution of the salinity of 121 cores taken from 0.22 m thick sea ice in a sheltered harbor in the Arctic, finding that the median salinity of samples was less than their mean. Winter-long time series of sea ice salinity, measured simultaneously with sea ice growth rate, are rare. In the Arctic, *Nakawo and Sinha* [1981] combined salinity and temperature measurements to investigate the effect of growth rate on first-year sea ice salinity and showed that the salinity at a given vertical position in the sea ice becomes stable (constant in time) from a few days after its formation until the sea ice warms in spring. In the Antarctic some winter first-year fast ice salinity series exist [*Günther and Dieckmann*, 1999; *Lei et al.*, 2010], but on each sampling occasion only one core

[1]Department of Physics, University of Otago, Dunedin, New Zealand.
[2]Geophysical Institute, University of Alaska Fairbanks, Fairbanks, Alaska, USA.
[3]National Institute of Water and Atmospheres Ltd., Wellington, New Zealand.
[4]Industrial Research Ltd., Lower Hutt, New Zealand.

0148-0227/12/2011JC007527

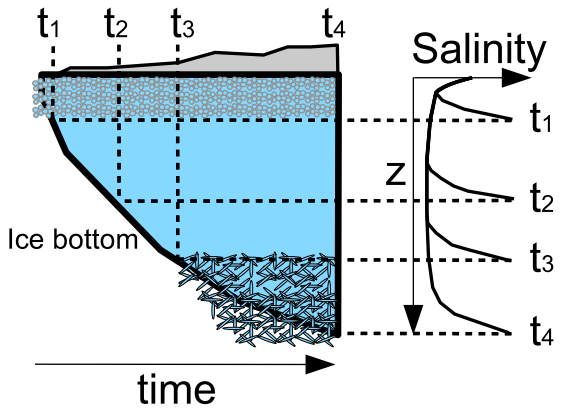

Figure 1. (left) Evolution of sea ice and its structure and (right) salinity profile at times t_1, t_2, t_3, and t_4 as a function of depth, z, near an ice shelf. Before t_1, frazil forms at the ocean surface and consolidates to form frazil ice. The ice bottom then advances, forming columnar ice ($t_1 \rightarrow t_2 \rightarrow t_3$). Once the ocean becomes supercooled (t_3), a porous subice platelet layer forms beneath the sea ice. Continued advance of the ice bottom consolidates this layer to form platelet ice ($t_3 \rightarrow t_4$).

was taken, so any changes in salinity over time cannot be separated from core-to-core variability.

[5] Clearly we might expect aspects of the permeability, and hence salinity, of sea ice to depend on the orientation of its component crystals. Ice crystals grow most rapidly along their basal plane. Once a sea ice cover has formed, continued growth selects crystals which can expand downward, so that ice crystals have a columnar character with their c axes oriented horizontally. Near ice shelves, supercooled water is known to emerge below the growing sea ice during the winter [e.g., *Leonard et al.*, 2006; *Mahoney et al.*, 2011], enhancing its growth by providing an additional sink for latent heat [*Purdie et al.*, 2006]. Eventually a porous matrix of disordered platelet crystals (called a subice platelet layer) is formed below the sea ice [*Smetacek et al.*, 1992]. Parts of this subice platelet layer can subsequently be subsumed by the advancing ice bottom to form platelet ice (see Figure 1) [e.g., *Lange*, 1988; *Eicken and Lange*, 1989; *Jeffries et al.*, 1993]. The crystals which form platelet ice show no preferred orientation, and display an isotropic distribution of their c axes [*Serikov*, 1963; *Paige*, 1966].

[6] The salinity of platelet ice has been studied less thoroughly than the more prevalent columnar ice. Some studies have taken a number of cores from platelet ice [e.g., *Eicken and Lange*, 1989; *Jeffries et al.*, 1993; *Gow et al.*, 1998; *Jones and Hill*, 2001; *Dempsey et al.*, 2010]. These were either geographically dispersed so that changes in forcings and uncertainty in the timing of initial ice formation make it difficult to directly compare one core with another, or were sampled so late in spring that the salinity profile may have changed because of the ice warming. Despite significant differences in structure, *Gow et al.* [1998] state that columnar and platelet ice appear to have similar salinities.

[7] Desalination is governed by the thermodynamic state of the sea ice, as well as the shape and connectivity of the brine inclusions (and hence the sea ice crystal structure). Our understanding of the mechanisms which drain and capture brine in sea ice is evolving [*Notz and Worster*, 2009]. Percolation theory suggests that we think of sea ice in terms of its microstructure [*Golden et al.*, 1998], and use the emergent properties of random networks to predict the behavior of sea ice at scales larger than the individual brine inclusions and pore connections. Percolation theory says little about the way brine leaves sea ice, but it does suggest there should be a critical threshold in brine volume fraction where permeability drops quickly to zero [*Golden et al.*, 2007]. Mushy layer theory treats the sea ice as a continuum, with the details of brine pores and tubes being included through the liquid fraction within a volume, while their transport properties are represented by a fluid permeability [*Worster and Wettlaufer*, 1997; *Feltham et al.*, 2006]. The equations of fluid dynamics and thermodynamics are then applied to determine the evolution of growing sea ice. Mushy layer theory has had some success in predicting the onset of convection in laboratory grown ice [*Worster and Wettlaufer*, 1997], reproduces some features of the sea ice salinity profile [*Notz and Worster*, 2009] and goes some way toward explaining the formation and distribution of brine channels [*Wells et al.*, 2011]. However, it is not yet possible to fully integrate the effects of gravity drainage [*Feltham et al.*, 2006; *Notz and Worster*, 2009], making it difficult to make predictions about sea ice salinity without employing parameterizations [e.g., *Vancoppenolle et al.*, 2010].

[8] In practice, sea ice models used in major climate simulations do not yet allow the sea ice salinity profile to evolve in a realistic way. The Los Alamos CICE model [*Bitz and Lipscomb*, 1999; *Hunke and Lipscomb*, 2010], for instance, uses a prescribed salinity profile typical of multiyear Arctic sea ice. Improved models, including those coupled to biological systems, are being produced and will inevitably find themselves introduced to the climate models of the future [*Vancoppenolle et al.*, 2007; *Tedesco et al.*, 2010]. Many are based on the work of *Cox and Weeks* [1988], who employed a thermodynamic scheme proposed by *Maykut and Untersteiner* [1971] and added parameterizations of brine segregation, drainage and expulsion to produce a salinity profile. Future development of models to represent the sea ice more realistically requires data against which model parameters and behavior can be tested [*Hunke et al.*, 2011].

[9] In this paper we will present salinity measurements taken by following established methods. Sea ice salinity is usually measured by extracting cores from the sea ice with a diameter of 7 to 10 cm, which is slightly smaller than the average brine channel spacing of 13.4 cm reported by *Lake and Lewis* [1970]. Once lifted to the surface, the core is sectioned and these segments are sealed in a pot or bag and transported to a laboratory where they are melted and their salinity is measured [*Eicken*, 2009]. Extracting a core inevitably leads to the loss of some brine from the sample, although this is less of a problem for parts of the sea ice which are cooler than about −5°C and so virtually impermeable [*Cox and Weeks*, 1983]. *Cox and Weeks* [1986] showed that sampling while the atmosphere above the sea ice is cold (<−10°C) will cause less than 1% of the brine within a sample to be expelled as the sample cools. Processing cores quickly minimizes errors from brine loss. Methods are emerging that make it possible to deduce sea ice salinity through nondestructive techniques, for instance

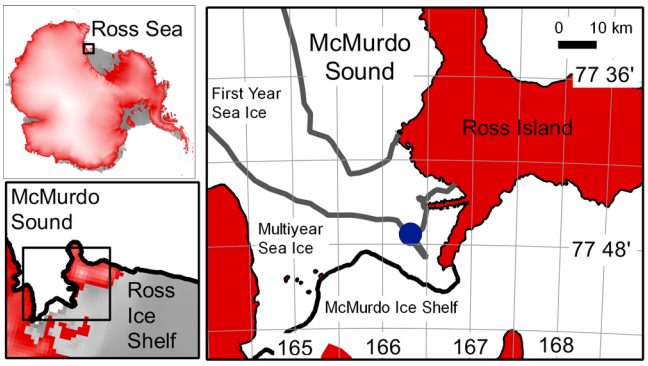

Figure 2. Our study site was located at 77°46.6′S, 166°18.8′E (blue dot) on an embayment of first-year sea ice within multiyear sea ice at the edge of the McMurdo Ice Shelf. Ice edge is from July 2009.

by measuring impedance using parallel wires [*Notz et al.*, 2005], complex dielectric permittivity using a Hydraprobe [*Backstrom and Eicken*, 2006] or through cross-borehole resistance measurements [*Ingham et al.*, 2008].

[10] The result of our study is a winter time series of sea ice salinity measurements from an area close to an ice shelf. We link these to measurements of sea ice growth rate and structure which are discussed in detail by *Gough et al.* [2012]. The prevailing oceanic conditions that drive changes in sea ice structure are discussed by *Mahoney et al.* [2011]. This new data set presented in this paper is sufficiently large that we explore the following.

[11] 1. We combine our salinity and growth rate data with those of *Nakawo and Sinha* [1981] and *Lei et al.* [2010] and test parameterizations of brine drainage suggested by a number of authors. The expected fluid flow regime within the permeable portions of the sea ice, using new measurements of the salinity profile immediately after initial freezing, is also investigated.

[12] 2. We demonstrate that the change in sea ice structure from columnar ice to platelet ice (see Figure 1) results in an increase in the salinity of the sea ice, provided that the effect of growth rate is removed. This suggests that the change in structure affects how brine is transported within sea ice.

[13] 3. We provide observations of the statistical distribution of horizontal and vertical variations in the salinity of typical first-year sea ice. This can be used as the prior distribution when interpreting sea ice salinity observations, and should be reproduced by sea ice models.

2. Study Area and Methods

[14] We sampled an area of first year sea ice in McMurdo Sound from soon after its formation in May 2009 until it reached a thickness of 2 m near the end of September 2009. The location of the site is shown in Figure 2.

[15] We will examine the salinity in 0.1 m vertical intervals, and obtain the average sea ice growth rate for each 0.1 m vertical interval using data from a mass balance site which was established in late May [*Gough et al.*, 2012]. Initially one, and later, three thermistor strings provided sea ice temperature measurements with vertical sensor spacing of between 0.03 m and 0.1 m. Temperature was measured with an accuracy of ±0.2°C or better. The location of the ice bottom, H (see Figure 1), was determined from core lengths, auger holes, hotwire gauges and temperature measurements (see *Gough et al.* [2012] for details). Our vertical coordinate, z, is zero at the snow-ice interface and positive upward, so H and dH/dt are negative as the ice grows downward. The dH/dt for each 0.1 m vertical interval of ice was calculated as the error-weighted mean of dH/dt determined from each method. As only interpolated drilled measurements were available while the ice was thin, the mean error in dH/dt for $H < 1$ m is 0.3 cm d^{-1} (for which $dH/dt > 1.25$ cm d^{-1}) while for $H > 1$ m the mean error is 0.05 cm d^{-1} (where $dH/dt < 1.25$ cm d^{-1}).

[16] Near the mass balance site an area 10 m by 25 m was marked out. Approximately every 2 weeks a group of three to six full thickness cores was extracted, with each core being at least 1 m from any other core's location, and each group of cores being separated by at least 2 m from any previous group of cores. Care was taken to avoid disturbance of the area still to be cored. Snow cover in the coring area changed over time but was uniform in thickness within 0.02 m for each group of cores taken. As each core was extracted it was scraped clean of shavings and quickly cut into segments 0.1 m long which were then sealed in clean plastic pots. Breaks in cores were reunited to form complete segments, with extraction of the next piece of core being timed so that cores were processed immediately after extraction. Temperature profiles were measured from these salinity cores but as salinity measurements were a priority these temperature measurements were taken by drilling 3 cm into the horizontal face of newly cut segments once they were placed in pots. Potted core samples were returned to Scott Base, melted, and their bulk salinity measured using a YSI-30 salinometer with an accuracy of ±0.1 in salinity. KCl standards were used to check that the salinometer did not drift from its calibration during the experiment.

[17] We refer to a measurement of salinity in each group (i.e., taken on a single day) g, from core i at level z using $S_{z,g,i}$. An approximate time line showing the number of cores in each group of cores from a given day is shown in Figure 3. All cores were 0.09 m diameter. By the end of the winter we had removed less than 1% of the sea ice

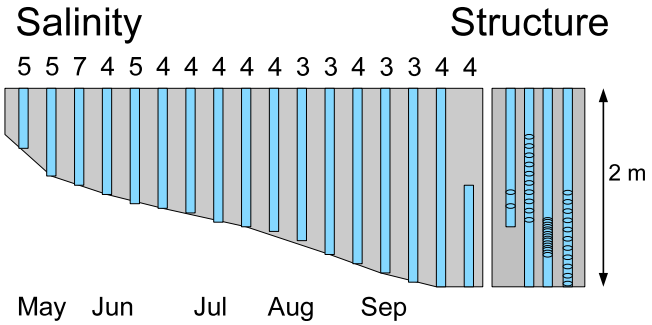

Figure 3. Field measurements presented in this paper. Over an area of 10 m × 25 m, 69 salinity cores were taken as the ice grew. The number of cores in each group is shown at the top. Four structural cores were taken at the end of the experiment. Small circles show the position of thin sections used to determine crystal orientations. The time axis is approximate.

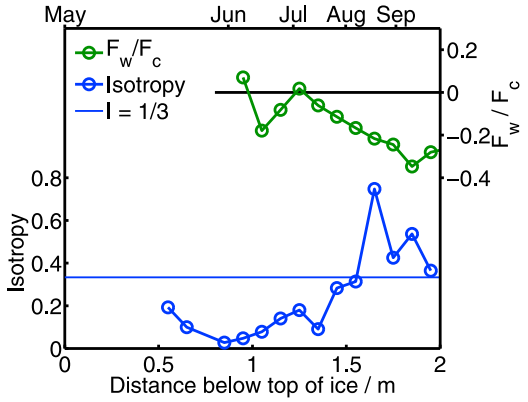

Figure 4. Heat flow and ice crystal structure at the ice bottom. (top) Ratio of F_w/F_c (green) from temperature strings [*Gough et al.*, 2012], where F_w is identified as the heat input to the ice from the ocean and F_c is the heat conducted upward within the sea ice. $F_w < 0$ implies the existence of an oceanic heat sink. (bottom) Isotropy of 0.1 m sections of sea ice. Columnar sea ice has $I \sim 0$. We select $I > 1/3$ to define platelet ice.

within the coring area, so any reduction in growth rate caused by our coring and the subsequent refreezing of holes will be no larger than 1%. This is confirmed by temperature measurements from cores that agreed with those measured by thermistor strings at the mass balance site.

[18] On three occasions (21 July and 14 and 21 September) a separate area was cored. The upper parts of the cores were discarded and the part of the core closest to the ice bottom was rapidly cut into segments 0.03 m or 0.04 m in thickness, starting from the lowest part of the core and working upward to minimize brine drainage for the most permeable ice. No temperature measurements were made on these cores. Air temperature on these occasions was always below −20°C. We refer to these cores later as "bottom cores" and use b to refer to a group of bottom cores, so that an individual measurement from a bottom core is $S_{z,b,i}$. Salinity was measured using the same procedure as the full-thickness cores.

[19] A final set of cores was taken from the full thickness of the ice for analysis of crystal structure. Cores were kept frozen below −20°C and processed in a cold laboratory at Scott Base. Thirty horizontal thin sections were made from a number of these cores. C axis measurements were made at approximately sixty points from each thin section using a universal stage as described by [*Langway*, 1958].

3. Measurement Results

[20] Let us begin by considering the crystal structure of the sea ice. We group c axis measurements from a given 0.1 m thickness of sea ice together. Measurements at a boundary between 0.1 m segments are included in the segment above the boundary, as the crystal fabric of the sea ice is shaped by the growth conditions prior to the formation of a given layer of the sea ice. For each segment we calculate an orientation tensor [*Woodcock*, 1977] and use this to determine an isotropy parameter, I [*Benn*, 1994]. $I \approx 0$ indicates the tendency of the crystal c axes to lie within the horizontal plane (typical of columnar ice), while $I \rightarrow 1$ implies that orientations of crystals are distributed randomly in all directions (typical of frazil ice, snow ice and platelet ice). We use this parameter to classify the ice as columnar ice ($I < 0.33$) or platelet ice ($I > 0.33$; see Figure 1). $I = 0.33$ corresponds to a texture where two thirds of the crystal c axes lie within 10° of the horizontal and one third are randomly distributed outside that band. This threshold also matches our visual impression of the ice texture, which is the usual way in which platelet ice is identified. In Figure 4 we show the evolution of the crystal structure over the winter as columnar ice is replaced by platelet ice at depths greater than 1.6 m. At timescales shorter than the 10 days it took for 0.1 m of sea ice to grow, this transition shows alternate layers of platelet and columnar ice from 1.5 m to 1.7 m, the details of which are discussed by *Gough et al.* [2012].

[21] Sea ice close to the ice bottom is permeable and continues to reject brine to the ocean. Once a permeability threshold has been passed brine will effectively be trapped within the sea ice for the remainder of the winter [*Nakawo and Sinha*, 1981; *Backstrom and Eicken*, 2006]. For each group of full-thickness cores, we determine the brine volume fraction (porosity), ϕ_l, at the time of coring using the warmest temperature within each 0.1 m segment, and the mean salinity profile from the group of cores, $\langle S_{z,g} \rangle$, derived from the relations given by *Cox and Weeks* [1983]. We discard all salinity measurements where $\phi_l > 0.054$ [*Petrich et al.*, 2006] in order to avoid time-dependent salinity changes. Using a nondestructive method, *Backstrom and Eicken* [2006] saw no change in the salinity of Arctic first year ice while ϕ_l remained below 0.06. Our results are unchanged if we vary this cutoff between possible values of 0.05 and 0.07 [*Petrich and Eicken*, 2007]. We use the symbol $S^\dagger$ for these "final" (time-independent) salinity measurements and $S^\dagger_{z,g,i}$, to indicate a particular measurement. Samples within 0.1 m of the ice-snow interface are also discarded from this analysis as they partially consist of small frazil crystals and partially of columnar crystals. In Figure 5 we plot $\langle S^\dagger_{z,g} \rangle - \langle S^\dagger_z \rangle$, the mean of each day's group of samples relative to the mean of all samples from each 0.1 m segment at depth z in the sea ice. While there is some variation from group to group, there is no significant change in either $\langle S^\dagger_{z,g} \rangle$ or the deviation of the measurements within each group over the sampling period, so salinity measurements from cores extracted early in the winter can be combined with those taken later in the winter.

[22] In Figure 6 we plot $S^\dagger_{z,g,i}$ against dH/dt determined from drill holes and temperature profiles; dH/dt is available only for measurements taken more than 0.4 m from the snow-ice interface. We see the expected trend in $S^\dagger$ with growth rate [e.g., *Kovacs*, 1996], and significant scatter about the mean salinity, with the maximum salinity at a given growth rate (vertical level in the sea ice) being up to 50% higher than the least saline sample. We also see that $S^\dagger$ of the platelet ice samples are higher than we would expect had the trend in $S^\dagger$ with dH/dt continued. This enhancement is small, with the mean of all platelet ice samples being 0.5 higher in salinity than that of the columnar ice samples with the closest (but higher) growth rate. The change in behavior is associated with the change in sea ice structure from columnar ice to platelet ice as $I > 0.33$ and not with the

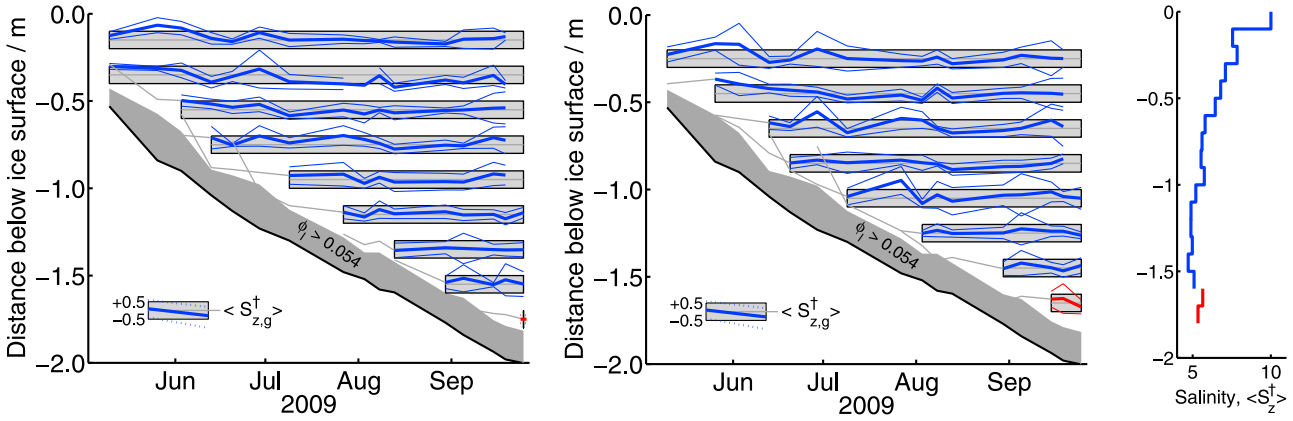

Figure 5. Salinity of 0.1 m layers of the sea ice over time. (left) Layers starting at $z = 0.2$ m, $z = 0.4$ m, etc. (middle) Layers starting at $z = 0.3$ m, $z = 0.5$ m, etc. Samples are not included if $\phi_l > 0.054$ (dark gray region). Thick black line shows the ice bottom. We plot the mean of cores taken each day relative to the mean from the whole winter's cores at that level: $\langle S^{\dagger}_{z,g} \rangle - \langle S^{\dagger}_z \rangle$. Thin lines show $\pm\sigma$ for each day's group of cores. Light gray bars have a height of 1 in salinity. Blue lines represent salinity for columnar ice ($I < 0.3$), and red lines are for platelet ice ($I > 0.3$). (right) The mean of all samples at each level, $\langle S^{\dagger}_z \rangle$.

change in the direction of the oceanic heat flux (F_w) at the ice bottom which occurs earlier (Figure 4). The platelet ice $S^{\dagger}$ lie within the scatter of columnar ice $S^{\dagger}$ with similar growth rates, so a study based on only one or two cores taken at the end of the growth season would not be expected to see this effect.

[23] Variability in the bulk salinity ($S^{\dagger}$) of sea ice is known to be driven by changes in the forcing conditions, such as air temperature and snow cover [*Eicken*, 1992]. At separations of a few meters these forcings should be constant and variations between cores should reflect the salinity field created by the processes by which the sea ice formed and developed. From Figure 6 it is clear that there is a significant spread in the individual measurements of $S^{\dagger}$ about the trend associated with dH/dt. One possible cause for the horizontal variation in salinity at a given vertical level in the ice is variations in the growth rate over horizontal separations of 1 to 2 m, perhaps through variations in the heat flux to or from the ocean. We can rule this out as a primary cause for two reasons: first, while we saw slightly different growth rates at each thermistor string at the mass balance site, we only ever saw a difference of <0.01 m in the length of sea ice cores taken on the same day, so any differences in growth rate must have been less than our measurement error. Second, looking at Figure 6, even a large change in growth rate will produce only a small change in salinity relative to the spread about the trend.

[24] To produce a single salinity distribution for all growth rates, we scale each final salinity measurement, $S^{\dagger}_{z,g,i}$, by the mean of all measurements at a given level, $\langle S^{\dagger}_z \rangle$ to produce a scaled salinity $S^{\star}_{z,g,i} = S^{\dagger}_{z,g,i} / \langle S^{\dagger}_z \rangle$. In Figure 7 we show the distribution of $S^{\star}_{z,g,i}$ for all measurements from full thickness cores, excluding those from the top 0.1 m of the sea ice as that was partially composed of frazil ice. The distribution is nonnormal, failing a Lilliefors test, but can be fitted well by a sum of two normal distributions:

$$P(S^{\star}) = pN_1(\mu_1, \sigma_1) + (1-p)N_2(\mu_2, \sigma_2) \quad (1)$$

where $N(\mu, \sigma)$ is a normal distribution with mean μ and standard deviation σ, and p weights the contribution of the first distribution. For our data, we find $p = 0.66 \pm 0.16$, $\mu_1 = 0.97 \pm 0.01$, $\sigma_1 = 0.05 \pm 0.01$, $\mu_2 = 1.06 \pm 0.04$, $\sigma_2 = 0.09 \pm 0.01$. Errors represent 95% confidence intervals, determined by bootstrapping with replacement of entire cores [*Efron and Tibshirani*, 1986]. The distribution is similar to that seen by *Weeks and Lee* [1962] for young, thin columnar ice with a median less than the mean, and a heavy tail toward higher salinities. This use of a sum of normals can be justified if the bulk salinity of the sea ice, when sampled at the scale of our corer, is formed from the contributions of two salinity fields (see Figure 7). One (N_1)

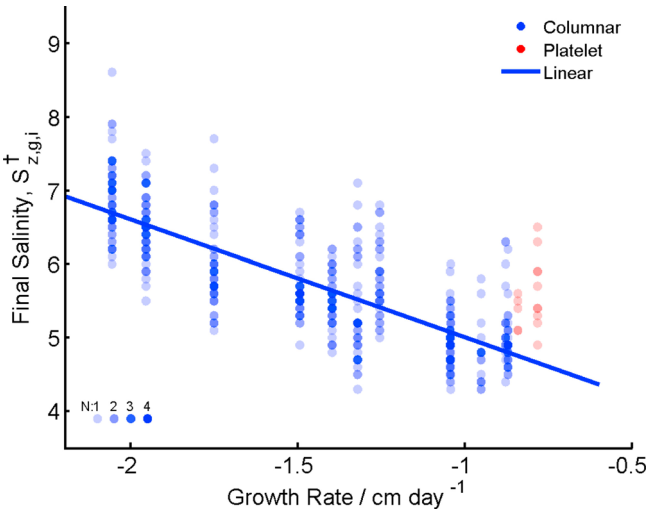

Figure 6. Salinity of columnar ice (blue) and platelet ice (red) for which $\phi_l < 0.054$ when sampled. All platelet ice salinities are above the linear trend, which is fitted only to the columnar ice samples. Shading indicates number of overlapping points.

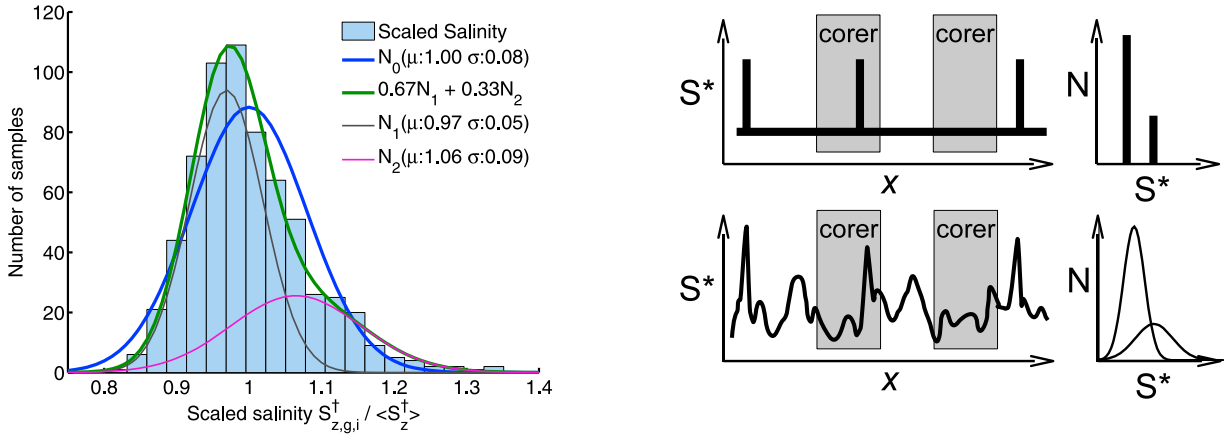

Figure 7. (left) Measurements of final salinity scaled by the mean of all measurements at the same level $S^{\star}_{z,g,i} = S^{\dagger}_{z,g,i}/\langle S^{\dagger}_{z}\rangle$. The distribution is not well described by a single normal distribution (N_0, blue line) but can be described by a mixture of two normal distributions (N_1 and N_2, green line). (right) A cartoon of the spatial fields that give rise to this distribution of scaled salinity. (top) With no variations, a background salinity combines with peaks caused by brine channels to produce a bimodal distribution. (bottom) Variations in the background salinity and in the width and intensity of brine channels produce a sum of normal distributions.

represents the background salinity of the sea ice with small-scale spatial variation, while a second contribution (N_2), associated with brine channels, produces vertical channels of enhanced salinity. These are then sampled by our corer to produce the final distribution seen in Figure 7. These two spatial fields could be produced by a single process, or through the interaction of a number of processes. We suggest that random variations in connectivity between brine tubes and pores leads to variations in the closing off of the pore network [*Golden et al.*, 1998] and so produces the intrinsic variability represented by N_1. At a larger scale, convection and the formation of brine channels leads to the tail of infrequent enhanced regions of salinity represented by N_2. We do not have enough measurements to determine if the distribution of salinity is different for different growth rates, or if platelet ice has a different distribution to columnar ice.

[25] This distribution can be used to test if two sets of measurements of quantities that are linearly related to the distribution of brine in sea ice are significantly different. We note that when comparing just two measurements of salinity at the same horizontal level in the sea ice, they must differ by 29% and 39% to be considered different at the 90% and 95% confidence levels, respectively. Our measurements are limited to growing, first-year sea ice at the end of winter, so a different distribution of salinity, and associated tracers, may result after the sea ice has begun to warm in spring. For instance, the mean standard deviation of salinity in thick undeformed multiyear sea ice (σ = 0.80) [*Untersteiner*, 1968] is higher than we measured here (σ = 0.46 for $S^{\dagger}$ = 6).

[26] It has been shown that brine channels are the primary driver of core-to-core variability in the salinity of sea ice [*Lake and Lewis*, 1970; *Tucker et al.*, 1984; *Cole and Shapiro*, 1998; *Cottier et al.*, 1999]. The link between the shape of brine drainage channels and the convective flows that control their formation is dramatically illustrated by the arch-shaped brine drainage features observed in refrozen cracks in sea ice [*Petrich et al.*, 2007]. To investigate the persistence of high or low salinity as the sea ice grows downward at a single location, we calculate the mean correlation within cores,

$$R_m = \frac{\left\langle \left(S^{\dagger}_{z,g,i} - \langle S^{\dagger}_{z}\rangle\right)\left(S^{\dagger}_{z+m,g,i} - \left\langle S^{\dagger}_{z+m}\right\rangle\right)\right\rangle}{\sigma_z \sigma_{z+m}} \qquad (2)$$

where m is the vertical separation between two samples in the ice and σ_z is the standard deviation of all $S^{\dagger}_{z,g,i}$ measurements at depth z. For a variable with a mean equal to its median, and distributed with no vertical correlation we expect R_m = 0. $S^{\dagger}$ has a mean greater than its median (Figure 7), so we would expect $R_m < 0$ if there were no vertical correlation between measurements.

[27] In Figure 8 we show R_m for vertical separations up to 1 m. The 95% confidence intervals for R_m were calculated using bootstrapping with replacement of entire cores [*Efron and Tibshirani*, 1986]. For vertically adjacent samples from the same core (m = 0.1 m) we find $R_m = 0.60 \pm 0.20$. Salinity measurements within a core remain correlated even for separations of 0.4 m where $R_m = 0.35 \pm 0.25$. This suggests that regions of enhanced or reduced $S^{\dagger}$ persist for at least 0.4 m vertically. If these are primarily caused by brine drainage features this becomes a good estimate of their vertical persistence and is similar to the length of brine channels of 0.3 to 0.5 m reported by *Cole and Shapiro* [1998] in Arctic sea ice. If one wishes to know the bulk properties of sea ice which are determined by its salinity or the distribution of tracers that are carried by the brine, taking measurements from a small number of cores may provide misleading information, even if samples are taken with a high vertical resolution, as cores are somewhat correlated.

[28] Measurements of salinity ($S_{z,b,i}$) from cores sectioned into pieces with vertical thickness of 2 cm or 3 cm from just above the ice-water interface are shown in Figure 9a. We also plot $\langle S^{\dagger}_{z}\rangle$ determined from full-thickness cores taken

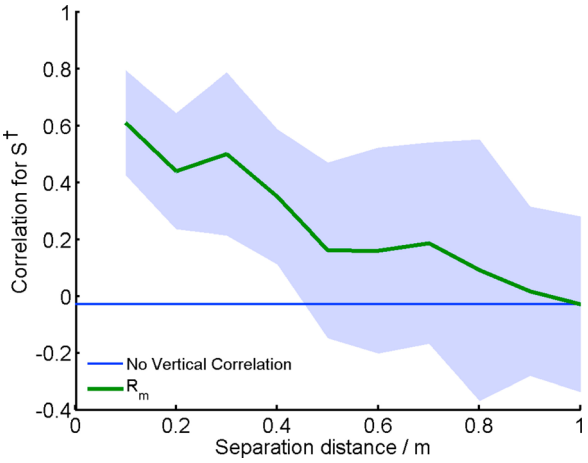

Figure 8. Correlation of salinity variations, $S^{\dagger}_{z,g,i} - \langle S^{\dagger}_{z,g,i} \rangle$, within cores at different vertical separations, m. We plot $R_m = \langle (S^{\dagger}_{z,g,i} - \langle S^{\dagger}_{z} \rangle)(S^{\dagger}_{z+m,g,i} - \langle S^{\dagger}_{z+m} \rangle) \rangle / \sigma_z \sigma_{z+m}$. The blue swath shows the 95% confidence interval. We also show R_m for simulated measurements with the same distribution of $S^{\dagger}$ as our measurements but with no vertical correlation.

later in the winter. For the groups below 1.8 m we do not have corresponding values of $\langle S_z \rangle$ as the porosity ϕ_l never dropped below our cutoff value.

4. Discussion of Salinity Profile

[29] In this section we discuss the processes which contribute to the shape of the mean vertical sea ice bulk salinity profile. We restrict our discussion to sea ice growing at an approximately constant rate, with a linear temperature profile near the freezing front which changes only slowly in time. We further assume there is no flushing of the sea ice with melt water so there is no net vertical brine velocity. These assumptions hold for the sea ice at our study site over the period for which we have temperature measurements [*Gough et al.*, 2012].

[30] Modern methods that simulate the evolution of sea ice salinity simplify the equations of mushy layer theory by modeling flushing processes (which we neglect) as Darcy flow, and convective processes (gravity drainage) as one-dimensional diffusive mixing (a "Reynold's flux," as outlined by *Jeffery et al.* [2011]).

[31] The one-dimensional sea ice bulk salinity profile then evolves as

$$\frac{\partial S}{\partial t} = \frac{\partial}{\partial z}\left(D^{\star} \frac{\partial S_{brine}}{\partial z} \right) \tag{3}$$

where S_{brine} is the brine salinity and $D^{\star}$ is an effective diffusion coefficient. A number of expressions for $D^{\star}$ have been proposed, with $D^{\star}$ being dependent on an effective mixing length, scaled from the molecular diffusivity [*Jeffery et al.*, 2011] or being some function of the local mushy layer Rayleigh number [*Vancoppenolle et al.*, 2010].

[32] If we assume that the system is in equilibrium, that there is a constant linear temperature gradient near the base of the sea ice and a linear liquidus relationship, $T = -\mu S_{brine}$, then equation (3) reduces to

$$\frac{\partial S}{\partial t} = -\frac{1}{\mu}\frac{\partial D^{\star}}{\partial z}\frac{\partial T}{\partial z} = G\frac{\partial T}{\partial z} \tag{4}$$

where we define $G = -\mu^{-1}\frac{\partial D^{\star}}{\partial z}$ for convenience later. We expect that, for the time it takes the sea ice to thicken by around 0.1 m, the salinity profile near the base of the sea ice will be a function of the distance above the freezing front, $S = S(z - H)$ (e.g., the deepest profiles in Figure 9a). Therefore, at a given vertical position in the sea ice,

$$\frac{\partial S}{\partial t} = -\frac{dH}{dt}\frac{\partial S}{\partial z} \tag{5}$$

so that,

$$G = -\frac{1}{\mu}\frac{\partial D^{\star}}{\partial z} = -\frac{\partial S}{\partial z}\frac{dH}{dt}\left(\frac{\partial T}{\partial z}\right)^{-1}. \tag{6}$$

[33] Using our bottom cores, dH/dt and dT/dz from *Gough et al.* [2012], taking $\mu = 0.054^{\circ}\mathrm{C\ psu^{-1}}$ [*Cox and Weeks*, 1983] and $S = 34.8$ [*Mahoney et al.*, 2011] at $z = H$

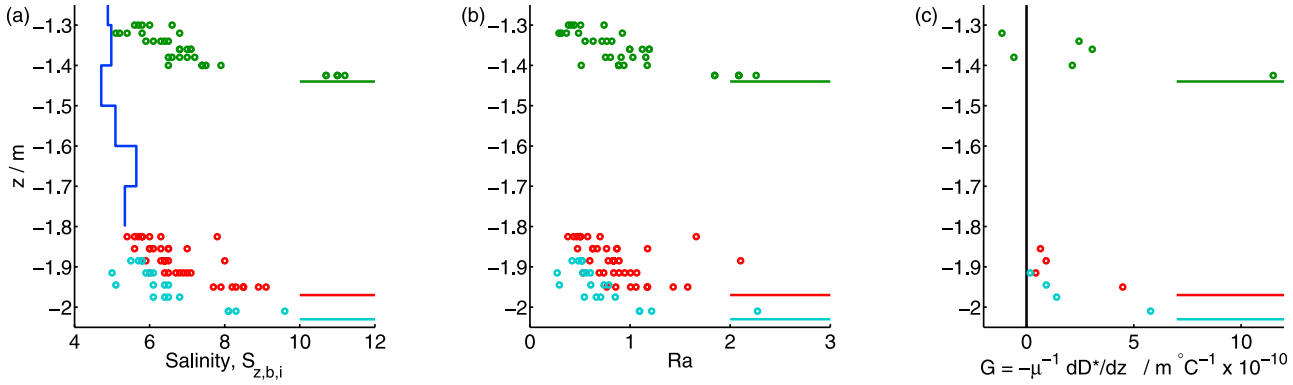

Figure 9. (a) Salinity, $S_{z,b,i}$, near the ice water interface on 21 July (green), 14 September (red), and 21 September (cyan); $\langle S^{\dagger}_{z} \rangle$ is shown in blue, where available. (b) Corresponding mushy layer Rayleigh number, Ra, and (c) strength of brine drainage, $G = -\mu^{-1}\partial D^{\star}/\partial z$. Horizontal lines show ice thickness, H, at each sampling time.

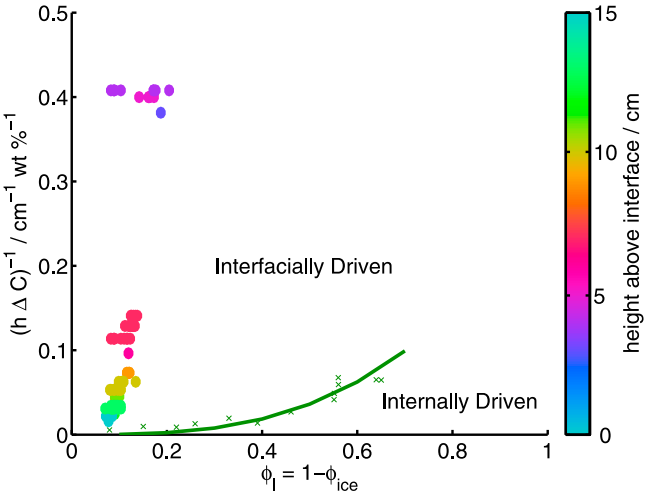

Figure 10. Plot of $(h\Delta C)^{-1}$ (h is distance above the ice bottom, and ΔC is the change in brine concentration from the sample to the ocean) against liquid fraction, ϕ_l, for samples from bottom cores, to which we have added contours of the mushy layer Rayleigh number (equation (7)). The green line, a fit to the measurements of *Wettlaufer et al.* [1997], delimits the change from an interfacial convective mode to a mode where convection cells penetrate the mushy layer at the base of the sea ice.

we calculate G near the base of the sea ice, as shown in Figure 9c. We see that G is larger near the freezing front, and decreases further into the sea ice. Since $D^\star$ must be small high up in the sea ice, this suggests, as expected, that the magnitude of the effective diffusivity is high near the freezing front where the liquid fraction, ϕ_l, is greatest, so that most brine is lost from the bottom few centimeters of the sea ice. Some brine may have drained from our samples during collection, especially those immediately at the ice-water interface, so our calculation of G will likely be an underestimate. Nevertheless, our measurements of salinity in the first few centimeters of the sea ice are consistent with those measured nondestructively by *Cox and Weeks* [1975].

[34] The diffusivity schemes sketched in equation (3) attempt to describe the mixing caused by convection within the sea ice, so it is useful to consider whether our measurements suggest that convection is occurring. Convection within a mushy layer is governed by the mushy layer Rayleigh number, Ra [*Wettlaufer et al.*, 1997; *Worster*, 1997; *Notz and Worster*, 2009]:

$$\mathrm{Ra} = \frac{g\beta(C_{brine} - C_{ocean})\Pi(\phi_l)h}{\kappa_{si}\nu} \qquad (7)$$

where g is the acceleration due to gravity, β is the volume expansion coefficient of brine, C_{brine} and C_{ocean} are the concentrations of salt in the brine and ocean, respectively, $\Pi(\phi_l)$ is the permeability of the sea ice, which is related to the liquid fraction (or brine volume fraction) ϕ_l of the sea ice, h is the vertical extent of the mushy layer, κ_{si} is the thermal diffusivity of sea ice and ν is the kinematic viscosity of brine. We take $\Pi(\phi_l)$ from *Freitag* [1999]. When Ra exceeds a critical value, Ra_c, of around 10, convection within the mushy layer is permitted [*Wettlaufer et al.*, 2000].

[35] In Figure 9b we show Ra for all individual core segments from our bottom cores, calculated using temperature profiles from nearby thermistor strings [*Gough et al.*, 2012] to determine C_b and ϕ_l [*Cox and Weeks*, 1983]. We take $h = z - H$ as the distance from the top of each sample to the ice bottom. We see that Ra lies around 2 in the segments at the ice-water interface, and drops to around 0.1 to 0.5 at $h = 0.1$ m. Profiles of both S, $-\frac{1}{\mu}\frac{\partial D^\star}{\partial z}$ and Ra are similar for columnar growth (21 July) and as sea ice advances into a subice platelet layer (14 and 21 September), suggesting that the processes causing brine to leave the sea ice are, broadly, unaffected by the structure of the sea ice.

[36] We can also use ideas from mushy layer theory to investigate the mode of convection occurring near the base of the sea ice. In Figure 10 we plot $(h\Delta C)^{-1}$ against the vertically averaged liquid fraction $\langle\phi_l\rangle = \langle 1 - \phi_{ice}\rangle$. We also plot measurements from [*Wettlaufer et al.*, 1997] of the transition from interfacial to internal convection in laboratory grown NaCl ice. *Worster and Wettlaufer* [1997] suggest that this transition represents a dynamic phase diagram for convection, with convection penetrating upward into the sea ice from the ice-water interface for points below their critical line. We see that all of our samples occupy the area above the critical line. While it is likely that some brine would drain from the sea ice during sampling of the bottom cores, we minimized this by sampling quickly in air temperatures that were below −20°C. It is unlikely that the true bulk salinity of the sea ice was such that our samples could lie anywhere but inside the area of Figure 10 in which internal convection is forbidden. This leads us to conclude that, for this thick, slowly growing first-year sea ice convection occurs at the interface in the boundary layer (or short-scale) mode. However, our points do lie close to a path on Figure 10, as one would expect if a Rayleigh number, which expresses the competition between buoyancy and viscous friction, was controlling brine drainage.

[37] The small values of Ra in Figure 9 are less than the critical value for convection of $Ra_c = 10$ [*Worster*, 1997]. This suggests that convection will not occur in the sea ice more than a few centimeters from the ice-water interface. The final salinity of the sea ice from full thickness cores, $\langle S_z^\dagger\rangle$, was lower than $\langle S_z\rangle$ for bottom cores at the same depth, implying that brine was still able to leave the sea ice (none of the bottom core segments had a porosity below our cutoff for $S^\dagger$ of $\phi_l < 0.054$). Internal convection at the base of the sea ice may occur only intermittently, which would require more variability in ice temperature than we saw with our thermistor strings, or brine may be lost from the sea ice through another mechanism.

[38] Such a mechanism may be provided by *Feltham et al.* [2002], who suggest that strong currents below the sea ice will generate ripples in the ice bottom and lead to horizontal pressure variations in the permeable sea ice close to the ocean. This leads to a reduction in the critical Rayleigh number for convection, and so may permit brine motion within the sea ice and its replacement with less saline sea water. Late in the winter, we observe a rough subice platelet layer below the sea ice which may decouple the sea ice near the ice bottom from the ocean. This reduces the effects of currents at the freezing front, perhaps explaining the small increase in $S^\dagger$ seen in Figure 6 when platelet ice forms, by

Table 1. Parameters Used to Drive a Simple Model of Sea Ice Desalination by Gravity Drainage, $dS/dt = A(\phi_l - \phi_{crit})^{\gamma} dT/dz$

Study	$A(\times 10^{-6}$ ppt m s^{-1} K$^{-1})$	ϕ_{crit}	γ	Reference
CW-88	3.37	0.05	1	*Cox and Weeks* [1988]
PLS-06	4.20	0.054	1.2	*Petrich et al.* [2006]
VBF-07	1.176	0.05	1	*Vancoppenolle et al.* [2007]
TVHS-10	11.76	0.05	1	*Tedesco et al.* [2010]

causing convection to halt at higher values of Ra [*Feltham et al.*, 2002]. However, some of our observations are not explained. For example the ice which formed immediately before a subice platelet layer, has an $S^{\dagger}$ as expected from the trend in $S^{\dagger}$ versus dH/dt (Figure 6). This ice must have been actively losing brine while a subice platelet layer was forming beneath it, and was presumably decoupled from the ocean in the same way, so it is not clear how important this "suction" mechanism is. A more complete understanding requires more observations.

5. Comparison With Basic Parameterizations

[39] We now further explore the enhanced $S^{\dagger}$ of platelet ice by comparing our measurements with predictions made by simple parameterizations which have been shown to work well for columnar sea ice. As the predictive capacity of the diffusion-based schemes outlined above is relatively untested we will use the basic parameterization of *Cox and Weeks* [1988] (CW-88) to simulate the salinity profile we would expect if no platelet ice was present. This scheme, and its variants, are widely deployed [e.g., *Eicken*, 1992; *Arrigo et al.*, 1993; *Petrich et al.*, 2006; *Vancoppenolle et al.*, 2007]. First we use our substantial data set to further test the applicability of CW-88 to columnar sea ice.

[40] In CW-88 the initial salinity of a newly formed layer of sea ice, S_{init}, varies with the rate of advance of the ice bottom through an effective segregation coefficient so that

$$S_{init} = S_0 K_{\mathrm{eff}} \left(\frac{dH}{dt} \right) \tag{8}$$

where S_0 is the ocean salinity and $K_{\mathrm{eff}}(dH/dt)$ is a segregation coefficient, a function of the growth rate. Measured values of $S_{z,b,i}$ (Figure 9a) from the portion of bottom cores closest to the ice bottom agree well with the expected values of S_{init}.

[41] The salinity of the sea ice layer then evolves through brine draining at a rate

$$\frac{dS}{dt} = A(\phi_l - \phi_{crit})^{\gamma} \frac{dT}{dz} \tag{9}$$

until the liquid fraction, $\phi_l < \phi_{crit}$. γ is a constant, usually 1, which allows for tuning of the strength of brine drainage. T is the sea ice temperature, and A is a constant. In effect they set

$$G = -\frac{1}{\mu} \frac{\partial D^{\star}}{\partial z} = A(\phi_l - \phi_{crit})^{\gamma} \tag{10}$$

in equation (4). In the CW-88 scheme, brine is also rejected from the sea ice as it is forced out through formation and expansion of the solid ice [*Cox and Weeks*, 1988, equation 4–7], but, as CW-88 stated, this expulsion term is generally much smaller than the drainage term. It is now believed that brine expulsion only internally redistributes small amounts of brine [*Notz and Worster*, 2009]. Once $\phi_l < \phi_{crit}$, S is no longer allowed to change so should correspond to our measurements of $S^{\dagger}$.

[42] More recently parameterizations have appeared where the constants used in the drainage term are changed from those initially determined by *Cox and Weeks* [1988]. *Petrich et al.* [2006] (PLS-06) reanalyzed the measurements of *Cox and Weeks* [1975] and found new values for their coefficients and changed the functional form of the drainage term by allowing $\gamma \neq 1$ in equation (9). *Vancoppenolle et al.* [2007] (VFB-07) produced a biologically coupled sea ice model (LIM1D) in which the coefficients were changed to better reproduce salinity profiles from a coastal site near Barrow, Alaska. The coefficients adopted in these schemes are shown in Table 1.

[43] The sea ice growth rate is determined by an energy balance at the ice-water interface:

$$-\rho_{si} L \frac{dH}{dt} = \left(-k \frac{dT}{dz} - F_w \right) = F_c - F_w \tag{11}$$

where ρ_{si} is the sea ice density, L the latent heat of formation [*Yen*, 1981], k the thermal conductivity of the sea ice [*Pringle et al.*, 2007], F_w accounts for heat supplied by the ocean, and F_c represents heat conducted upward by the sea ice. As we are interested in simulating sea ice growing at a constant velocity, we fix dH/dt and F_w and use equation (11) to find the required temperature gradient in the sea ice.

[44] A small layer of sea ice at time t after the freezing front has passed has temperature:

$$T(t) = T_{ocean} - \frac{dT}{dz} \frac{dH}{dt} t \tag{12}$$

with T_{ocean} approximately constant.

[45] During our observations both dH/dt and dT/dz near $z = H$ changed slowly (for -1.1 m $> H > -1.8$ m, -1.15 cm d$^{-1} < dH/dt < -.85$ cm d^{-1} [*Gough et al.*, 2012]). Thus, we simulate sea ice growing at constant velocity and with a constant imposed temperature gradient near the base of the sea ice. We take typical values for $k = 2.2$ W m^{-2} K^{-1} and $L = 3.4 \times 10^5$ J kg^{-1} (for sea ice with $T = -10$°C and $S = 6$) and $\rho = 930$ kg m^{-3} [*Timco and Frederking*, 1996] and model coefficients from Table 1.

[46] In Figure 11 we plot S_f from these simulations along with $S^{\dagger}$ from our study. We also show $S^{\dagger}$ from winter-long measurements in the Arctic by [*Nakawo and Sinha*, 1981] and the Antarctic by *Lei et al.* [2010]. From these published studies we have interpolated salinity profiles to produce

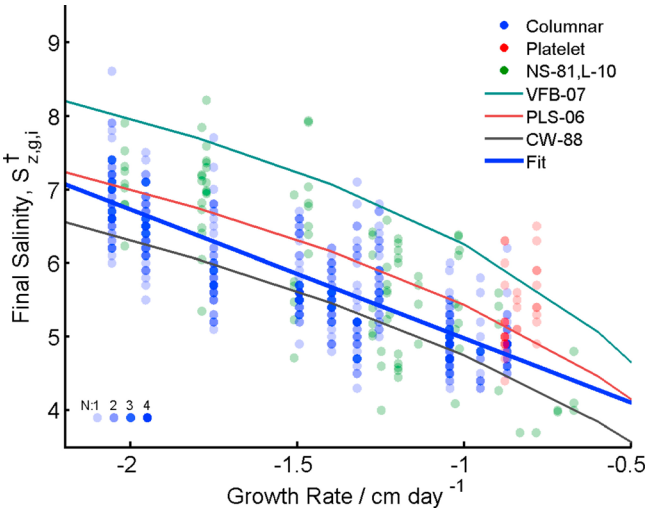

Figure 11. Salinity of sea ice from this study (blue and red) and from winter-long studies by *Nakawo and Sinha* [1981] (NS-81) and *Lei et al.* [2010] (L-10), with salinity and growth rate averaged into 0.1 m intervals. The linear trend (Fit) for all nonplatelet samples is also shown. Lines show model results using coefficients from Table 1. CW-88 and PLS-06 lie close to the trend but do not predict higher salinity for platelet ice. TVHS-10 lies below the bottom of the figure.

segments 0.1 m in height, and have selected measurements using the criteria employed in our study. The constants adopted by *Tedesco et al.* [2010] (TVHS-10) lead to a significantly higher rate of brine drainage than required as they were tuned to correctly produce thin, slowly growing sea ice. We see that both the unmodified CW-88 scheme and that of *Petrich et al.* [2006] (PLS-06) reproduces the mean salinity of the data well, and that our platelet ice measurements show enhanced $S^{\dagger}$ when compared with both the shape of the models, and with the other studies in which platelet ice was not present.

[47] In these CW-88 schemes, the same path will be taken in [S, T] space no matter what the magnitude and direction of heat fluxes at the base of the sea ice, so that S_f only depends on the resulting growth rate. This is clearly contrary to our results in Figure 6, as dH/dt did not change significantly while F_w became more negative and platelet ice replaced columnar ice (see Figures 4 and 6) but the salinity of the platelet ice was higher than that measured for the columnar ice. We therefore ask if G should depend somehow on the structure of the sea ice.

[48] The mushy layer Rayleigh number is dependent on the permeability of the sea ice. This is taken to be a simple function of the porosity of the sea ice, $\Pi(\phi_l)$, but this relationship may also be dependent on the structure of the sea ice. The disordered crystals in platelet ice may cause the brine network to be less well connected vertically but better connected horizontally than in columnar ice. If the vertical component of permeability controls convection [e.g., *Petrich et al.*, 2006] then this could lead to the observed enhancement of salinity in platelet ice. In the view of percolation theory, where $\Pi \sim (\phi_l - \phi_{crit})^{\alpha}$, with $\alpha \approx 3$, we would expect this reduction in connectedness to cause the critical porosity, ϕ_{crit}, at which permeability becomes negligible, to occur at a higher porosity for platelet ice than for normal columnar ice.

6. Conclusion

[49] Platelet ice consists of large crystals with isotropic c axis orientations while columnar ice is composed of crystals with predominantly horizontal c axes. For the first time we establish that, once growth rate is accounted for, platelet ice has a slightly higher salinity than columnar ice. This may be caused by decreased permeability in platelet ice, probably because of changes in the connectivity of the microstructure of the sea ice, requiring the adoption of a structure-dependent permeability-porosity relationship. Nevertheless, the increase in salinity is still small, requiring a large number of measurements to be detectable, even though the structure of platelet ice is significantly different. This suggests that the mechanisms which drain brine from growing sea ice must be broadly unaffected by the details of the microstructure.

[50] We attempted to apply a Rayleigh number criterion to our measurements of sea ice salinity close to the ice bottom as there is a paucity of natural data suitable for comparison. The permeability of sea ice is not well known, especially for high brine volume fractions. This makes it difficult to interpret the results of applying Rayleigh number criterion to our observations. Methods to measure fluid permeability or other aspects of the microstructure in situ are desirable.

[51] We note that the growth of thick sea ice can be modeled with a constant growth rate and a linear temperature profile near the base of the sea ice. Future schemes for desalination can be forced in this way and compared with our data. By combining our data with those from similar studies, we have demonstrated that the mean salinity of thick columnar sea ice at the end of winter can be adequately predicted using the original parameterization of *Cox and Weeks* [1988] or its modified form [*Petrich et al.*, 2006]. These parameterizations, though, do not function so well where platelet ice is present.

[52] We show that deviations from the mean salinity profile persist for at least 0.4 m vertically, in effect making a core of 1 m of sea ice consist of only two or three independent measurements. Any measurement taken from a single core should not be subjected to too much interpretation.

[53] Finally we provide a significant set of new data describing first-year sea ice salinity at the end of its period of growth. This yields a distribution of salinity when sampled by a 90 mm corer, reflecting the variability seen over only a few meters horizontally. Efforts to model and predict the salinity of growing sea ice should attempt to reproduce the shape of this distribution and to explain the sources of this variability. Our distribution of scaled salinity can now be used to inform statistical tests when comparing one set of sea ice measurements with another.

[54] **Acknowledgments.** This work, part of New Zealand's contribution to the IPY, was funded by the Foundation for Research Science and Technology and a University of Otago postgraduate scholarship. Antarctica New Zealand provided logistical support. We thank Brian Staite and the 2009 Scott Base wintering team for valuable assistance in the field. We are grateful to Craig Purdie for advice while planning this experiment and Inga Smith and Chris Petrich for comments that improved this paper. Some temperature data were provided by Joe Trodahl. The comments of two anonymous reviewers significantly improved this paper.

References

Arrigo, K. R., J. N. Kremer, and C. W. Sullivan (1993), A simulated Antarctic fast ice ecosystem, *J. Geophys. Res.*, *98*(4), 6929–6946.

Assur, A. (1958), Composition of sea ice and its tensile strength, in *Arctic Sea Ice*, *Natl. Res. Counc. Publ.*, *598*, 106–138.

Backstrom, L. G. E., and H. Eicken (2006), Capacitance probe measurements of brine volume and bulk salinity in first-year sea ice, *Cold Reg. Sci. Technol.*, *46*(3), 167–180.

Benn, D. I. (1994), Fabric shape and the interpretation of sedimentary fabric data, *J. Sediment. Res., Sect. A*, *64*(4), 910–915.

Bennington, K. O. (1967), Desalination features in natural sea ice, *J. Glaciol.*, *6*(48), 845–857.

Bitz, C. M., and W. H. Lipscomb (1999), An energy-conserving thermodynamic model of sea ice, *J. Geophys. Res.*, *104*(C7), 15,669–15,677.

Cole, D. M., and L. H. Shapiro (1998), Observations of brine drainage networks and microstructure of first-year sea ice, *J. Geophys. Res.*, *103*(C10), 21,739–21,750.

Cottier, F., H. Eicken, and P. Wadhams (1999), Linkages between salinity and brine channel distribution in young sea ice, *J. Geophys. Res.*, *104*(C7), 15,859–15,871, doi:10.1029/1999JC900128.

Cox, G. F. N., and W. F. Weeks (1975), Brine drainage and initial salt entrapment in sodium chloride ice, *Res. Rep. ADA021765*, 85 pp., Cold Reg. Res. and Eng. Lab., Hanover, N. H.

Cox, G. F. N., and W. F. Weeks (1983), Equations for determining the gas and brine volumes in sea-ice samples, *J. Glaciol.*, *29*(102), 306–316.

Cox, G. F. N., and W. F. Weeks (1986), Changes in the salinity and porosity of sea-ice samples during shipping and storage, *J. Glaciol.*, *32*(112), 371–375.

Cox, G. F. N., and W. F. Weeks (1988), Numerical simulations of the profile properties of undeformed first-year sea ice during the growth season, *J. Geophys. Res.*, *93*(C10), 12,449–12,460.

Dempsey, D. E., P. J. Langhorne, N. J. Robinson, M. J. M. Williams, T. G. Haskell, and R. D. Frew (2010), Observation and modeling of platelet ice fabric in McMurdo Sound, Antarctica, *J. Geophys. Res.*, *115*, C01007, doi:10.1029/2008JC005264.

Efron, B., and R. Tibshirani (1986), Bootstrap methods for standard errors, confidence intervals, and other measures of statistical accuracy, *Stat. Sci.*, *1*(1), 54–75.

Eicken, H. (1992), Salinity profiles of Antarctic sea ice: Field data and model results, *J. Geophys. Res.*, *97*(C10), 15,545–15,557.

Eicken, H. (2009), Ice sampling and basic sea ice core analysis, in *Field Techniques for Sea Ice Research*, p. 117–140, Univ. of Alaska Press, Fairbanks.

Eicken, H., and M. A. Lange (1989), Development and properties of sea ice in the coastal regime of the southeastern Weddell Sea, *J. Geophys. Res.*, *94*(C6), 8193–8206, doi:10.1029/JC094iC06p08193.

Eicken, H., C. Bock, R. Wittig, H. Miller, and H.-O. Poertner (2000), Magnetic resonance imaging of sea-ice pore fluids: Methods and thermal evolution of pore microstructure, *Cold Reg. Sci. Technol.*, *31*, 207–225.

Eide, L. I., and S. Martin (1975), The formation of brine drainage features in young sea ice, *J. Glaciol.*, *15*(70), 137–154.

Feltham, D. L., M. G. Worster, and J. S. Wettlaufer (2002), The influence of ocean flow on newly forming sea ice, *J. Geophys. Res.*, *107*(C2), 3009, doi:10.1029/2000JC000559.

Feltham, D. L., N. Untersteiner, J. S. Wettlaufer, and M. G. Worster (2006), Sea ice is a mushy layer, *Geophys. Res. Lett.*, *33*, L14501, doi:10.1029/2006GL026290.

Freitag, J. (1999), Untersuchungen zur hydrologie des Arktischen meereises Konsequenzen fur den kleinskaligen stofftransport, *Ber. Polarforsch.*, *325*, 1–170.

Golden, K. M., S. F. Ackley, and V. I. Lytle (1998), The percolation phase transition in sea ice, *Science*, *282*, 2238–2241, doi:10.1126/science.282.5397.2238.

Golden, K. M., H. Eicken, A. L. Heaton, J. Miner, D. J. Pringle, and J. Zhu (2007), Thermal evolution of permeability and microstructure in sea ice, *Geophys. Res. Lett.*, *34*, L16501, doi:10.1029/2007GL030447.

Gough, A. J., A. Mahoney, P. J. Langhorne, M. J. M. Williams, N. J. Robinson, and T. G. Haskell (2012), Signatures of supercooling: McMurdo Sound platelet ice, *J. Glaciol.*, *58*(207), 38–50, doi:10.3189/2012JoG10J218.

Gow, A., S. Ackley, J. Govoni, and W. Weeks (1998), Physical and structural properties of land-fast sea ice in McMurdo Sound, Antarctica, in *Antarctic Sea Ice: Physical Processes, Interactions and Variability*, *Antarct. Res. Ser.*, vol. 74, edited by O. Jeffries, pp. 355–374, AGU, Washington, D. C.

Günther, S., and G. S. Dieckmann (1999), Seasonal development of algal biomass in snow-covered fast ice and the underlying platelet layer in the Weddell Sea, Antarctica, *Antarct. Sci.*, *11*, 305–315.

Hunke, E. C., and W. H. Lipscomb (2010), CICE: The Los Alamos sea ice model documentation and software user's manual (version 4.1), *Tech. Rep. LA-CC-06-012*, T-3 Fluid Dyn. Group, Los Alamos Natl. Lab., Los Alamos, N. M., May.

Hunke, E. C., D. Notz, A. K. Turner, and M. Vancoppenolle (2011), The multiphase physics of sea ice: A review, *Cryosphere*, *5*, 989–1009, doi:10.5194/tc-5-989-2011.

Ingham, M., D. Pringle, and H. Eicken (2008), Cross-borehole resistivity tomography of sea ice, *Cold Reg. Sci. Technol.*, *52*(3), 263–277.

Jeffery, N., E. C. Hunke, and S. M. Elliott (2011), Modeling the transport of passive tracers in sea ice, *J. Geophys. Res.*, *116*, C07020, doi:10.1029/2010JC006527.

Jeffries, M., W. Weeks, R. Shaw, and K. Morris (1993), Structural characteristics of congelation and platelet ice and their role in the development of Antarctic land-fast sea ice, *J. Glaciol.*, *39*, 223–238.

Jones, S. J., and B. T. Hill (2001), Structure of sea ice in McMurdo Sound, Antarctica, *Ann. Glaciol.*, *33*(1), 5–12.

Kovacs, A. (1996), Sea ice part I. Bulk salinity vs. ice-floe thickness, *Rep.96-7*, Cold Reg. Res. and Eng. Lab., Hanover, N. H.

Lake, R. A., and E. L. Lewis (1970), Salt rejection by sea ice during growth, *J. Geophys. Res.*, *75*(3), 583–597, doi:10.1029/JC075i003p00583.

Lange, M. A. (1988), Basic properties of Antarctic sea ice as revealed by textural analysis of ice cores, *Ann. Glaciol.*, *10*, 95–101.

Langway, C. (1958), Ice fabrics and the universal stage, *Tech. Rep. 62*, U.S. Army Snow, Ice and Permafrost Res. Establ., Wilmette, Ill.

Lei, R., Z. Li, B. Cheng, Z. Zhang, and P. Heil (2010), Annual cycle of landfast sea ice in Prydz Bay, east Antarctica, *J. Geophys. Res.*, *115*, C02006, doi:10.1029/2008JC005223.

Leonard, G. H., C. R. Purdie, P. J. Langhorne, T. G. Haskell, M. J. M. Williams, and R. D. Frew (2006), Observations of platelet ice growth and oceanographic conditions during the winter of 2003 in McMurdo Sound, Antarctica, *J. Geophys. Res.*, *111*, C04012, doi:10.1029/2005JC002952.

Mahoney, A. R., A. J. Gough, P. J. Langhorne, N. Robinson, C. Stevens, M. J. M. Williams, and T. Haskell (2011), The seasonal appearance of ice shelf water in coastal Antarctica and its effect on sea ice growth, *J. Geophys. Res.*, *116*, C11032, doi:10.1029/2011JC007060.

Malmgren, F. (1927), On the properties of sea ice, in *Scientific Results of the Norwegian North Pole Expedition With the Maud 1919–1925*, vol. 1a, pp. 1–67, John Griegs, Bergen, Norway.

Maykut, G. A., and N. Untersteiner (1971), Some results from a time-dependent thermodynamic model of sea ice, *J. Geophys. Res.*, *76*(6), 2–4.

Nakawo, M., and N. K. Sinha (1981), Growth rate and sea ice salinity profile of first-year sea ice in the high Arctic, *J. Glaciol.*, *27*(96), 315–330.

Niedrauer, T. M., and S. Martin (1979), An experimental study of brine drainage and convection in young sea ice, *J. Geophys. Res.*, *84*(C3), 1176–1186, doi:10.1029/JC084iC03p01176.

Notz, D., and M. G. Worster (2009), Desalination processes of sea ice revisited, *J. Geophys. Res.*, *114*, C05006, doi:10.1029/2008JC004885.

Notz, D., J. S. Wettlaufer, and M. G. Worster (2005), A non-destructive method for measuring the salinity and solid fraction of growing sea ice in situ, *J. Glaciol.*, *51*(172), 159–166.

Paige, R. A. (1966), Crystallographic studies of sea ice in McMurdo Sound, Antarctica, *Tech. Rep. R-494*, U.S. Naval Civ. Eng. Lab., Idaho Falls, Idaho.

Petrich, C., and H. Eicken (2007), Growth, structure and properties of sea ice, in *Sea Ice*, pp. 23–77, Wiley-Blackwell, Oxford, U. K.

Petrich, C., P. J. Langhorne, and Z. F. Sun (2006), Modelling the interrelationships between permeability, effective porosity and total porosity in sea ice, *Cold Reg. Sci. Technol.*, *44*(2), 131–144.

Petrich, C., P. J. Langhorne, and T. G. Haskell (2007), Formation and structure of refrozen cracks in land-fast first-year sea ice, *J. Geophys. Res.*, *112*, C04006, doi:10.1029/2006JC003466.

Pringle, D. J., H. Eicken, H. J. Trodahl, and L. G. E. Backstrom (2007), Thermal conductivity of landfast Antarctic and Arctic sea ice, *J. Geophys. Res.*, *112*, C04017, doi:10.1029/2006JC003641.

Purdie, C., P. J. Langhorne, G. Leonard, and T. Haskell (2006), Growth of first-year landfast Antarctic sea ice determined from winter temperature measurements, *Ann. Glaciol.*, *44*, 172.

Serikov, M. I. (1963), Structure of Antarctic sea ice, *Sov. Antarct. Exped. Inf. Bull., Engl. Transl.*, *39*, 13–14.

Smetacek, V., R. Scharek, L. I. Gordon, H. Eicken, E. Fahrbach, G. Rohardt, and S. Moore (1992), Early spring phytoplankton blooms in ice platelet layers of the southern Weddell Sea, Antarctica, *Deep Sea Res., Part A*, *39*(2), 153–168.

Tedesco, L., M. Vichi, J. Haapala, and T. Stipa (2010), A dynamic biologically active layer for numerical studies of the sea ice ecosystem, *Ocean Modell.*, *35*(1-2), 89–104.

Timco, G. W., and R. M. W. Frederking (1996), A review of sea ice density, *Cold Reg. Sci. Technol.*, *24*(1), 1–6.

Tucker, W. B., A. J. Gow, and J. A. Richter (1984), On small-scale horizontal variations of salinity in first-year sea ice, *J. Geophys. Res.*, *89*(4), 6505–6514, doi:10.1029/JC089iC04p06505.

Untersteiner, N. (1968), Natural desalination and equilibrium salinity profile of perennial sea ice, *J. Geophys. Res.*, *73*(4), 1251–1257, doi:10.1029/JB073i004p01251.

Vancoppenolle, M., C. M. Bitz, and T. Fichefet (2007), Summer landfast sea-ice desalination at Point Barrow Alaska: Modeling and observations, *J. Geophys. Res.*, *112*, C04022, doi:10.1029/2006JC003493.

Vancoppenolle, M., H. Goosse, A. de Montety, T. Fichefet, B. Tremblay, and J.-L. Tison (2010), Modeling brine and nutrient dynamics in Antarctic sea ice: The case of dissolved silica, *J. Geophys. Res.*, *115*, C02005, doi:10.1029/2009JC005369.

Weeks, W. F. (2010), *On Sea Ice*, Univ. of Alaska Press, Fairbanks.

Weeks, W. F., and O. S. Lee (1962), The salinity distribution in young sea-ice, *Arctic*, *15*(2), 93–108.

Weissenberger, J., G. Dieckmann, R. Gradinger, and M. Spindler (1992), Sea ice: A cast technique to examine and analyze brine pockets and channel structure, *Limnol. Oceanogr.*, *37*(1), 179–183.

Wells, A. J., J. S. Wettlaufer, and S. A. Orszag (2011), Brine fluxes from growing sea ice, *Geophys. Res. Lett.*, *38*, L04501, doi:10.1029/2010GL046288.

Wettlaufer, J. S., M. G. Worster, and H. E. Huppert (1997), Natural convection during solidification of an alloy from above with application to the evolution of sea ice, *J. Fluid Mech.*, *344*, 291–316.

Wettlaufer, J. S., M. G. Worster, and H. E. Huppert (2000), Solidification of leads: Theory, experiment, and field observations, *J. Geophys. Res.*, *105*(C1), 1123–1134, doi:10.1029/1999JC900269.

Woodcock, N. (1977), Specification of fabric shapes using an eigenvalue method, *Geol. Soc. Am. Bull.*, *88*, 1231–1236.

Worster, M. G. (1997), Convection in mushy layers, *Annu. Rev. Fluid Mech.*, *29*, 91–122.

Worster, M. G., and J. S. Wettlaufer (1997), Natural convection, solute trapping, and channel formation during solidification of saltwater, *J. Phys. Chem. B*, *101*(96), 6132–6136.

Yen, Y. (1981), Review of thermal properties of snow, ice and sea ice, *Tech. Rep. 81-10*, U. S. Army Cold Reg. Res. and Eng. Lab., Hanover, N. H.

A. J. Gough and P. J. Langhorne, Department of Physics, University of Otago, Dunedin 9016, New Zealand. (ajgo@physics.otago.ac.nz)

T. G. Haskell, Industrial Research Ltd., 69 Gracefield Rd., PO Box 31310, Lower Hutt 5040, New Zealand.

A. R. Mahoney, Geophysical Institute, University of Alaska Fairbanks, Fairbanks, AK 99709, USA.

M. J. M. Williams, National Institute of Water and Atmospheres Ltd., Private Bag 14901, Wellington, New Zealand.